Physics-Lumped Parameter Based Control Oriented Model of Dielectric Tubular Actuator

Theophilus Kaaya · Shengbin Wang · Marzia Cescon · Zheng Chen*

Received: date / Accepted: date

Abstract Dielectric elastomers (DEs) deform and change shape when an electric field is applied across them. They are flexible, resilient, light weight, and durable and as such are suitable for use as soft actuators. In this paper a physicsbased and control-oriented model is developed for DE tubular actuator using a physics-lumped parameter modeling approach. The model derives from the nonlinear partial differential equations (PDE) which governs nonlinear elasticity of the DE actuator and the ordinary differential equation (ODE) which governs the electrical dynamics of the DE actuator. With the boundary conditions for tubular actuator, the nonlinear PDEs are numerically solved and a quasi-static nonlinear model is obtained and validated by experiments. The full nonlinear model is then linearized around an operating point with an analytically derived Hessian matrix. The analytically linearized model is validated by experiments. Proportional–Integral–Derivative (PID) and H_{∞} control are developed and implemented to perform position reference tracking of the DEA and the controllers' performances are evaluated according to control energy and tracking error.

Keywords Dielectric elastomer actuator \cdot Tubular actuator \cdot Finite Element \cdot Control

1 INTRODUCTION

Dielectric elastomer actuators (DEAs), a class of electro active polymers, offer promising properties over conventional actuators in that they are compact and do not require a large amount of space to operate [1]. They are flexible and as such

Department of Mechanical Engineering, University of Houston, 4726 Calhoun Rd, Houston, TX 77204

Tel.: +1713-743-6427

 $\label{eq:constraint} E-mail: tskaaya@uh.edu (TK), swang62@uh.edu(SW), \\ mcescon2@uh.ed (MC), zchen43@central.uh.edu (ZC).$

*Corresponding author: Zheng Chen.

can be molded to take up different shapes yet still offer good performance due to the fact that the performance is primarily influenced by the elastomer prestretch, mechanical stiffness, permittivity, and compliant electrodes [2]. They can be made to be resilient and durable able to reach large linear actuation strains and maintain good performance for many cycles of actuation [3]. They are also quiet and hence reduce noise pollution under operation compared to conventional rigid actuators. Due to their low noise production, DEAs can be employed in many research areas such as marine and aquatic research to effectively study fish and marine life with minimal interference [4]. In their simplest configuration, they are easy to manufacture and the material is readily available [5–8]. The actuators are light-weight, which means that they can be carried easily for instance on an individual's body, in generators, and loud speakers [9]. In addition, they offer large amounts of strain when a voltage is applied across the membranes of the actuators. They have a high elastic energy density that can be harnessed to produce large deformations and electric generation [10]. The DEAs are also called artificial muscles used to mimic the movement of muscles in the design of bionic robots and in prostheses to help disabled people recover their movement and function of lost limbs [11, 12]. The DEA's performance and characteristics render them ideal in soft robotics. Current work on dielectric tubular actuators has found its application in refreshable braille displays [13], push actuators [14], and active vibration isolation [15] to mention but a few.

With all these benefits however, the dielectric actuators are challenging to model and their behavior is unpredictable in certain configurations [16]. To analyze the dynamics of the actuators, circuit based models have been devised along with frequency based models that capture the actuator's dynamics [17–20]. These methods ignore the actual physics of the actuators and as such do not explain in effect the coupling between the mechanical and electrical quantities of the

actuator as well as its geometry as a whole. Most physics model based work depends on static based analysis of the actuators. The dynamic analysis on the other hand involves the use of rheological models to account for the the viscoelastic behaviour of the actuators. In this paper the quasi static model is extended into a dynamic model to analyze the dynamics of the actuator. The advantage of a physics model is its ability to describe how material properties and the actuator's geometry affect the dynamics and behavior of the actuator under different states [21]. The lumped parameter model accounts for the physical quantities that are not fully expressed when formulating the physics based model.

The control of these actuators is also still challenging and is an area of open research [22]. Previous work by G Rizzello *et al* [23] and Zhihang Ye *et al* [24] successfully implemented PID and H_{∞} control respectively on a diaphragm DEA. This paper intends to apply the same controls on the tubular DEA and compare the performance of the controllers. Other types of control have been implemented such as adaptive control and sliding mode control [25,26] to mention but a few.

Different configurations exist for dielectric actuators such as stacked, diaphragm, rolled, and tubular [27–30]. In this paper a physics-lumped parameter based model of the tubular dielectric actuator is presented which can be used to predict and control the deformation of the DEA. The derivation process follows closely that of Tianhu He *et al.* [31] with modifications made specific to the tubular dielectric actuator. The distinction here is that the tubular actuator membrane varies longitudinally while the diaphragm actuator membrane for He varies radially. As a result one of the equations of state changes to reflect the change in geometry. Furthermore, a bridge is made between the field of material science to that of control systems by converting the quasi static model to a dynamic model through the algebraic equation.

One of the main contributions of this paper is the introduction of a methodology in solving the differential equations that arise from the physics of the actuator to ensure that physical values, that is, positive stretch values of the actuator, are accounted for in solving the equations. As will be seen in the following discussion, the longitudinal stretch of the actuator is solved from a quartic algebraic equation which poses a challenge of having four solutions to the stretch. Instead of solving the roots of the algebraic equation each time, the equation is transformed into a differential equation to track the locus of the positive stretch value of the actuator. The challenge of solving three ordinary differential equations (ODEs) with a constraint is thus transformed to one of solving four ODEs without constraints. This approach ensures one unique solution for the tubular actuator given the fact that the shooting method, which may potentially produce multiple solutions, is used to arrive at the desired solution.

Secondly, a bridge is made between the quasi-static model and the dynamic model from which one can observe the interaction or influence the physical parameters have on the system model. Since the dynamic model is derived from the algebraic equation, a fictitious damping coefficient is introduced into the system by taking the derivative of the algebraic equation with velocity to account for the viscoelasticity of the actuator. This forms the physics-lumped parameter model of the actuator. This interaction cannot be observed when a black-box model is used in the control of the actuator since the model structure identified by this method is not unique. Lastly, an attempt is made to determine the linearized model parameter coefficients of the actuator analytically. This allows for fast adjustment and model update when the operating point of the actuator changes removing the need to run experiments each time in identifying these values.

The rest of the paper is organized as follows: Section 2 discusses a nonlinear quasi-static elastic model of the tubular DEA along with its simulation and validation. Section 3 presents the dynamic model, analytical parameter identification, and model identification developed from the quasistatic model using frequency response analysis. Section 4 discusses the control system design using PID and H_{∞} . Section 5 discusses experimental results for the tubular actuator with the designed controllers. Finally, section 6 discusses the conclusion and future work.

2 Modeling of tubular DEA

2.1 The quasi-static model

In this section, the governing equations that describe the shape and behavior of the tubular actuator are derived. Figure 1 shows a cross-section of the tubular actuator in the undeformed state (a) and deformed state (b).

In the current configuration, the actuator is fixed at the top and free to move at the bottom. The actuator is given a pre-stretch in the longitudinal direction (X-axis) by attaching a weight at the bottom. The attached weight has significant effects on the behavior of the actuator since it shifts the actuator from one mode (state) to another. Consider specific points (particles) on the membrane at A and at B. The particles at A are constrained by the fixed top disk and do not move during actuation. The particles at B are free to move vertically but are constrained by the bottom disk with the disk radius R. All other points on the membrane are located at the radius R and the depth X forming the reference coordinate system (X,R) where R is fixed in the undeformed state. A general particle p at (X,R) in figure 1(a) moves to a location (r,z) in the current coordinate system (figure 1(b)) when a vertical force F, or an applied voltage Φ , or both are exerted onto the membrane.

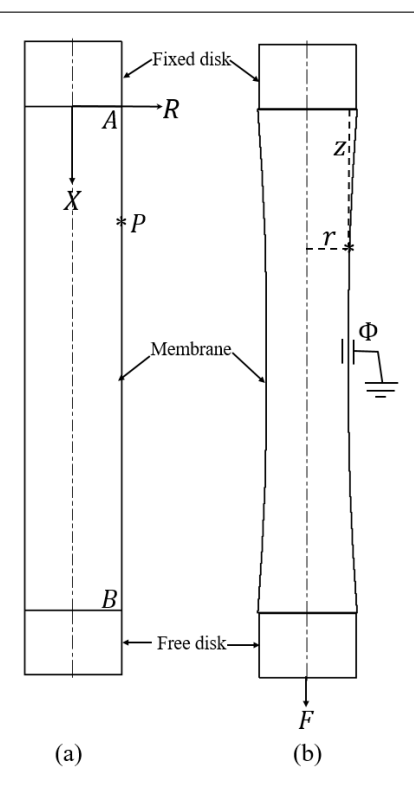


Fig. 1 Cross section of tubular actuator in undeformed state (a), and deformed state (b).

Consider an element on the actuator with one end at (X,R) and another at (X+dX,R) where dX is the elemental length in the undeformed state. This ends undergo deformation to occupy the new locations (r(X),z(X)) and (r(X+dX),z(X+dX)) respectively. Let the particles in the deformed state be separated by a distance dl forming an angle θ with the horizontal measured from the second point counterclockwise. This produces a change in r and in z, which is given by

$$dr = r(X + dX) - r(X)$$
 and $dz = z(X + dX) - z(X)$.

Since the orientation of the element changes with X, then

$$dr = -dl\cos(\theta),$$
 $dz = dl\sin(\theta),$ (1)

where θ is taken as the angle of the element with respect to the horizontal. For this element,

$$dl^2 = dr^2 + dz^2. (2)$$

The geometry of the actuator is thus fully described.

To characterize the mechanical and electrical components of the actuator, three parameters are defined: The longitudinal stretch (along the X-axis), λ_1

$$\lambda_1 = \frac{dl}{dX} = \sqrt{\left(\frac{dr}{dX}\right)^2 + \left(\frac{dz}{dX}\right)^2},\tag{3}$$

the latitudinal (circumferential) stretch, λ_2

$$\lambda_2 = \frac{2\pi r}{2\pi R} = \frac{r}{R},\tag{4}$$

and the nominal charge density, \bar{D}

$$\bar{D} = \frac{q}{A_0},\tag{5}$$

where q is the charge on the element and A_0 is the elemental area in the undeformed state. These three parameters λ_1 , λ_2 , and \bar{D} fully describe the deformation of the actuator under an applied load F and/or voltage Φ . The total charge Q on the actuator is given as

$$Q = 2\pi R \int \bar{D}dX. \tag{6}$$

Since the actuator relies on the ability of the dielectric membrane to undergo large strain deformations, Helmholtz's energy, E_H is used to describe the energy of the actuator as

$$E_H = 2\pi R H \int W dX, \tag{7}$$

where W is the nominal Helmholtz's energy assumed to be a function of λ_1 , λ_2 , and \bar{D} . H is the thickness of the membrane in the undeformed state. For a small change in λ_1 , λ_2 , and \bar{D} , the Helmholtz's energy undergoes a change

$$\delta W = s_1 \delta \lambda_1 + s_2 \delta \lambda_2 + \bar{E} \delta \bar{D}, \tag{8}$$

where

$$s_1 = \frac{\partial W}{\partial \lambda_1}, s_2 = \frac{\partial W}{\partial \lambda_2}, \bar{E} = \frac{\partial W}{\partial \bar{D}}.$$
 (9)

 s_1 , s_2 , and \bar{E} are the longitudinal nominal stress, the circumferential nominal stress, and the nominal electric field respectively.

In a state of equilibrium, the change in the Helmholtz's energy of the actuator is equal to the work done in moving the actuator from one state to another through the work done by the applied force and voltage. Therefore

$$\delta E_H = 2\pi R H \int \delta W dX = F \, \delta z_B + \Phi \, \delta Q, \tag{10}$$

also

$$\int \delta W dX = \int (s_1 \delta \lambda_1 + s_2 \delta \lambda_2 + \bar{E} \delta \bar{D}) dX, \tag{11}$$

where

$$\delta \lambda_1 = -\cos(\theta) \frac{d(\delta r)}{dX} + \sin(\theta) \frac{d(\delta z)}{dX}, \tag{12}$$

$$\delta \lambda_2 = \frac{\delta r}{R}, \qquad \delta \bar{D} = \frac{\delta q}{A_0}.$$
 (13)

To this end, solving Eq. 11 over the entire length of the actuator from *A* to *B* and substituting into Eq. 10 give

$$\frac{d(s_1\cos\theta)}{dX} = -\frac{s_2}{R},\tag{14}$$

$$2\pi R H s_1 \sin \theta = F,\tag{15}$$

$$H\bar{E} = \Phi. \tag{16}$$

Eq. 14 to 16 are the equations of state of the actuator.

For the material model of the actuator, the actuator is assumed to be an ideal incompressible dielectric elastomer. In assuming in-compressibility, the stretch in the thickness direction is given by $\lambda_3=1/\lambda_1\lambda_2$. For the ideal actuator, the dielectric property of the actuator is not affected by deformation hence the dielectric constant, ε_r is assumed to be fixed. For simplicity, a neo-hookean model [32] is chosen to characterize the actuator's free-energy density. Other models such as the Yeoh model [33], and the Ogden model [34] may be employed to get more accurate results that cover larger strains in the actuator. The neo-hookean model is given by

$$W(\lambda_1, \lambda_2, \bar{D}) = \frac{\mu}{2} (\lambda_1^2 + \lambda_2^2 + \lambda_1^{-2} \lambda_2^{-2} - 3) + \frac{\bar{D}^2}{2\varepsilon} \lambda_1^{-2} \lambda_2^{-2},$$
(17)

where μ is the shear modulus of the actuator and ε the permittivity of the membrane. From Eq. 17, Eq. 9 is solved to obtain

$$s_1 = \mu(\lambda_1 - \lambda_1^{-3}\lambda_2^{-2}) - \frac{\bar{D}^2}{\varepsilon}\lambda_1^{-3}\lambda_2^{-2},\tag{18}$$

$$s_2 = \mu(\lambda_2 - \lambda_2^{-3}\lambda_1^{-2}) - \frac{\bar{D}^2}{\varepsilon}\lambda_2^{-3}\lambda_1^{-2},\tag{19}$$

$$\bar{E} = \frac{\bar{D}}{\epsilon} \lambda_1^{-2} \lambda_2^{-2}.\tag{20}$$

To investigate this model, the differential equations that characterize the shape of the actuator as well as the mechanical and electrical properties of the actuator are normalized as follows: The applied load as $F^*=F/2\pi H\mu$, the applied voltage $\Phi^*=\Phi/(H\sqrt{\mu/\varepsilon})$, the vertical deformed position $z^*=z/L$, and the radial deformation $r^*=r/R$. Eq. 1 and Eq. 3 give

$$\frac{dr}{dX} = -\lambda_1 \cos \theta, \qquad \frac{dz}{dX} = \lambda_1 \sin \theta. \tag{21}$$

Differentiating Eq. 15 with respect to X and combining it with Eq. 14 give

$$\frac{d\theta}{dX} = \frac{s_2}{s_1 R} \sin \theta. \tag{22}$$

Finally the algebraic equation from Eq. 15 can be written as

$$\left[1 - \left(\frac{\Phi^* r}{R}\right)^2\right] \lambda_1^4 - \frac{F^*}{R\sin(\theta)} \lambda_1^3 - \left(\frac{R}{r}\right)^2 = 0.$$
 (23)

Eq. 21–23 form the governing equations of the tubular actuator.

2.2 Simulation of tubular DEA Model

The algebraic equation is analyzed to establish the number of permissible stretch values of λ_1 . It is worth noting that the stretch must be a positive value at all times since this is a physical system. Let

$$A = \left[1 - \left(\frac{\Phi^* r}{R}\right)^2\right], \quad B = \frac{F^*}{R\sin(\theta)}, \quad C = \left(\frac{R}{r}\right)^2.$$

such that the algebraic equation becomes

$$A\lambda_1^4 - B\lambda_1^3 - C = 0. (24)$$

It can be seen that for the tubular actuator described above, B and C can never have a sign change since for B the interval for θ is (0,90]. On the other hand, A can have a sign change if

$$\left(\frac{\Phi^*r}{R}\right)^2 > 1.$$

This condition can be used to find the maximum allowable theoretical voltage that may be applied on the actuator before it breaks down. It is required that *A* be positive at all times. Using Routh Hurwitz stability criterion [35],

$$\lambda_1^4 \quad A \quad 0 - C
\lambda_1^3 \quad -B \quad 0 \quad 0
\lambda_1^2 \quad \varepsilon - C
\lambda_1^1 \quad \frac{-BC}{\varepsilon}
\lambda_1^0 \quad -C$$
(25)

It can be observed that the elements above and below the ε in the first column have the same sign therefore a pair of imaginary roots exist in the algebraic equation. There is also a single sign change which implies that there is always one positive root whenever A is positive. The fourth remaining root is therefore negative. From this observation the requirement for keeping A positive at all times can be justified. This observation is useful when running the numerical simulation as it is the basis used to keep track of the positive root locus of the algebraic equation when solving the differential equations. To track this root, the algebraic equation is differentiated with respect to X to end up with

$$\frac{d\lambda_{1}}{dX} = \frac{-\frac{F^{*}\cos\theta\lambda_{1}^{3}}{R\sin^{2}\theta} \cdot \frac{d\theta}{dX} - 2\left[\frac{R^{2}}{r^{3}} - r\left(\frac{\Phi^{*}}{R}\right)^{2}\lambda_{1}^{4}\right]\frac{dr}{dX}}{\left(4\left[1 - \left(\frac{\Phi^{*}r}{R}\right)^{2}\right]\lambda_{1} - \frac{3F^{*}}{R\sin\theta}\right)\lambda_{1}^{2}}.$$
 (26)

The four differential equations 21, 22, and 26 can now be solved numerically. Considering the boundary conditions, solving these PDEs becomes a two boundary valued problem with the boundaries being r(0) = r(L) = R where L is the total length of the actuator in the undeformed state. z(0) = 0 but z(L) as well as $\theta(0)$, $\theta(L)$ and $\lambda_1(0)$ are unknown. In order to establish $\lambda_1(0)$ the algebraic equation

needs to be solved given r(0) and $\theta(0)$. As such, the PDEs are solved using the shooting method in which an initial guess of $\theta(0)$ that satisfies the two boundary conditions r(0) = r(L) = R is made.

The value of the shear modulus is chosen and calibrated to closely fit the experimental data collected for multiple applied loads. Since the model used is the Neo-Hookean model, it is important that the correct shear modulus of the actuator is chosen to accurately predict the displacement. It should be noted that the shear modulus is a function of temperature and frequency of actuation of the actuator attributed to the viscous effect of the VHB (Very High Bond) tape [36]. VHB (3M) is an acrylic elastomer that is used as the dielectric elastomer of choice for the DEA throughout this paper. The simulation is run with F = 20 gf (gram-force) and $\Phi = 0$ V. This particular simulation is performed using MATLAB R2019a [37]. For a given $\theta(0)$, the positive value of $\lambda_1(0)$ is calculated by solving the roots of the algebraic equation and choosing the positive root. This value is the one that is then used to solve Eq. 26 and with this, each iteration of the numerical simulation ensures that λ_1 is always positive since the starting value of the iteration is positive. With r(0), $\theta(0)$, z(0), and $\lambda_1(0)$, the rest of the differential equations are solved using ode45() to produce r(X), z(X), $\theta(X)$, and $\lambda_1(X)$. Post processing is performed on these variables such as estimating the behavior and trend of displacement vs applied voltage and displacement vs load. Figure 2 and Fig. 3 show these trends respectively. Furthermore the model can be used to perform closed loop control as is discussed in section 3.

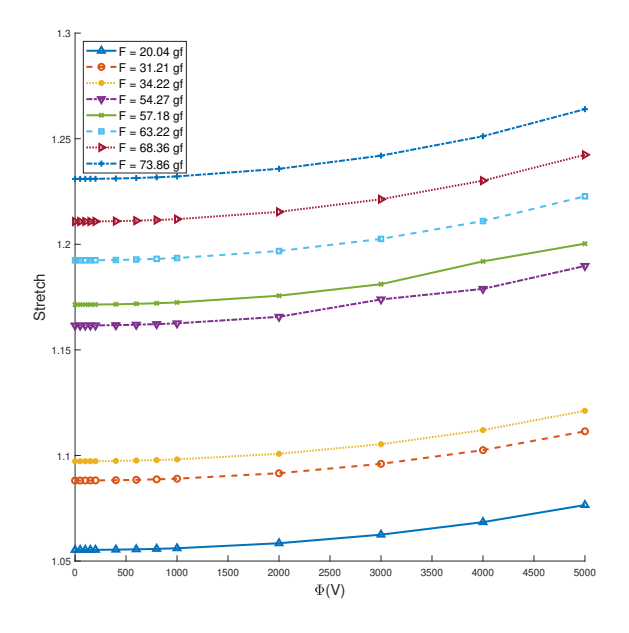


Fig. 2 Simulation of stretch vs Applied voltage.

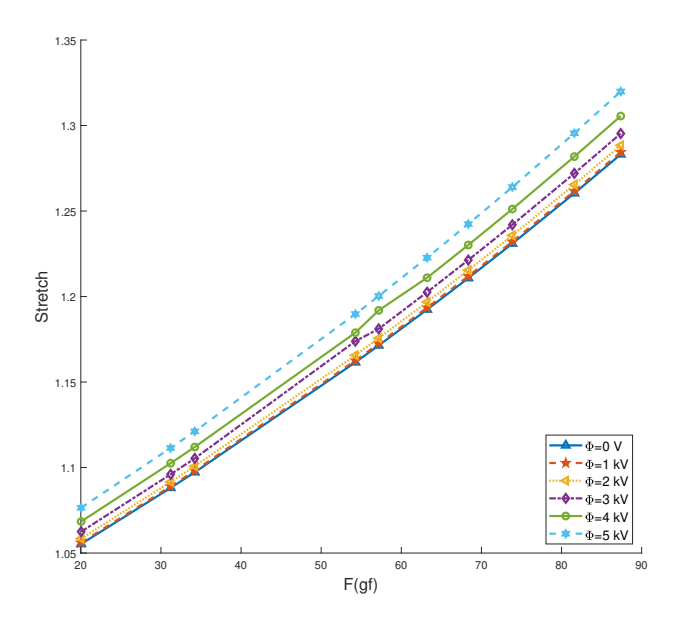


Fig. 3 Simulation of stretch vs applied load.

2.3 Quasi-static Model Validation

The geometrical parameters of the tubular DEA used in the simulation are shown in Table 1 below. The actuator is made

Table 1 Geometry parameters for simulation and validation

Parameter	Value	Unit
Radius	20.66	(mm)
Thickness	1	(mm)
Height	78	(mm)

from 3M VHB 4910 material of 130 cm by 78 cm size cut from a tape roll. The VHB is rolled and attached onto two plastic cylinders. One acts as the support (fixed end) while the other is free to move (bottom end). The ends of the membrane are covered with insulating tape to prevent short circuit between the two electrodes one on the outer side of the membrane and the other on the inner side of the membrane. Carbon grease(MG Chemicals) is used as the compliant electrode and is pasted on both sides of the DE membrane uniformly. A load of 20.04 gf is fixed on the bottom end of the actuator producing a strain of 3.846 %. The final length of the DE tube is 81 mm. The experimental setup is shown in Figure 4(a). The data for the actual shape of the DEA is extracted from the image using image digitizing software and compared with the simulated shape. A comparison is shown in Figure 4(b).

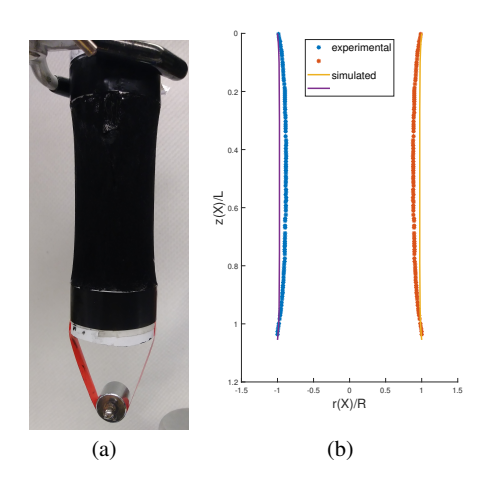


Fig. 4 Experimental validation. (a) Experimental setup; (b) Experimental vs simulated shape.

It may be observed that the actual shape curvature is more pronounced than the simulation. The model is also tested on how well it predicts the displacement of the actuator with various weights. Figure 5 shows a comparison between the experimental and simulated displacements with various weights applied on the actuator.

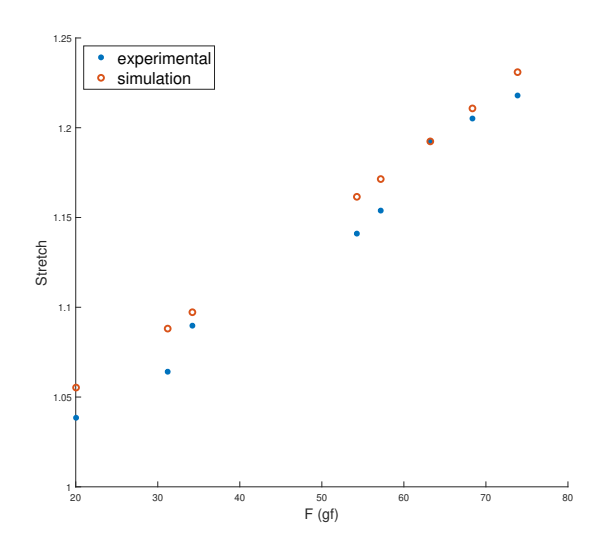


Fig. 5 Experimental vs simulated stretch.

As may be observed, the model does not account for the viscous effects in the actuator so it provides the final equilibrium displacement of the DEA while the experimental data has to go through the transient stages in order to reach the equilibrium state for an applied load. Table 2 shows the error between the predicted and experimental displacements for various weight values. The model, though simple can

Table 2 Percentage error for displacement prediction for various loads

F (gf)	20.04	31.21	34.22	54.27
Error(%)	1.62	2.26	0.69	1.80
F (gf)	57.18	63.22	68.36	73.86
r (gr)	37.10	03.22	00.50	75.00

predict the displacement of the tubular actuator and its sensitivity can be tuned to perform well around a given fixed load.

3 Dynamic model of the DEA

3.1 State Space Model of DE Tubular Actuator

A dynamic model is developed from the quasi-static model established in section 2 using the theory of elasticity and electrostatics by rewriting the algebraic equation and combining it with Newton's second law of motion. To account for viscous effects that are not captured by the quasi-static model, a lumped parameter damping is introduced into the force balance of the actuator. The acceleration of the actuator is given by

$$a^* = g^* - \frac{R\sin(\theta)}{m\lambda_1^3} \left(\left[1 - \left(\frac{\Phi^* r}{R} \right)^2 \right] \lambda_1^4 - \left(\frac{R}{r} \right)^2 \right) - \frac{c^*}{m} v, \tag{27}$$

where $a^* = a/2\pi H\mu$ is the normalized acceleration, $g^* = g/2\pi H\mu$ the normalized gravity, $c^* = c/2\pi H\mu$ the normalized damping coefficient, and v the velocity of the actuator. Taking the total stretch as $\lambda_i = \lambda_i^a \lambda_i^p$ with λ_i^a as the stretch due to actuation, λ_i^p the pre-stretch due to the added weight, and i = 1, 2, 3, the acceleration can be written as

$$\begin{split} a^* &= \frac{R \sin \theta}{m (\lambda_1^p)^3} \Bigg\{ (1 - \lambda_1^a) (\lambda_1^p)^4 + \left(\frac{1}{(\lambda_2^a)^2 (\lambda_1^a)^3} - 1 \right) \frac{1}{(\lambda_2^p)^2} \\ &\quad + \left(\Phi^* r \lambda_2^a \lambda_2^p \right)^2 \lambda_1^a (\lambda_1^p)^4 \Bigg\} - \frac{c^*}{m} v. \end{split}$$

Assuming small pre-stretch, $\lambda_i^p \approx 1$, the acceleration may be rewritten to include only the actuated stretch terms

$$a^* = -\frac{R\sin(\theta)}{m\lambda_1^3} \left(\left[1 - \left(\frac{\Phi^* r}{R} \right)^2 \right] \lambda_1^4 - \left(\frac{R}{r} \right)^2 \right) - \frac{c^*}{m} v, \tag{28}$$

where λ_i^a is replaced with λ_i for neatness.

Eq. 23 is rewritten to serve as the spring for the actuator. Treating the actuator as a classic RC circuit for simplification purposes, a relationship between the driving normalized

voltage, u^* , and the normalized voltage on the membrane, Φ^* , is given by

$$\dot{\Phi}^* = -\frac{\Phi^*}{RC} + \frac{u^*}{RC},$$

where R is the circuit resistance and C is the membrane capacitance and

$$u^* = \frac{u}{H} \sqrt{\frac{\varepsilon}{\mu}}.$$

Let x_1 be the position of the bottom disk of the actuator and $v = x_2 = \dot{x}_1$ the velocity. Then its acceleration is $a^* = \ddot{x}_1 = \dot{x}_2$. Finally let $x_3 = \Phi^*$, which gives the dynamic model of the tubular actuator as Eq. 21, 22 and

$$\dot{x}_{1} = x_{2}, \tag{29}$$

$$\dot{x}_{2} = -\frac{R\sin(\theta)}{m\lambda_{1}^{3}} \left(\left[1 - \left(\frac{x_{3}r}{R} \right)^{2} \right] \lambda_{1}^{4} - \left(\frac{R}{r} \right)^{2} \right) - \frac{c^{*}}{m} x_{2}, \tag{30}$$

$$\dot{x}_3 = -\frac{x_3}{RC} + \frac{u^*}{RC}. (31)$$

The dynamics is evaluated at the equilibrium point where the tubular actuator settles under a constant mechanical load. At this point, the model is linearized. In order to complete linearization, note that r, z, θ , and λ_1 are also functions of x_1 , x_3 , and time t. Assuming small perturbations about the equilibrium point and that the shape of the actuator does not change significantly for small actuation, the first three differential equations may be ignored which helps reduce the order of the system to leave behind three states (x_1, x_2, x_3) . Linearization introduces an error in the model and is accounted for using the model uncertainty ΔG to ensure that the controllers developed remain stable around the equilibrium point. The Jacobian, J of the system takes the form

$$\mathbf{J} = \begin{bmatrix} \frac{\partial \dot{x}_1}{\partial x_1} & \frac{\partial \dot{x}_1}{\partial x_2} & \frac{\partial \dot{x}_1}{\partial x_3} \\ \frac{\partial \dot{x}_2}{\partial x_1} & \frac{\partial \dot{x}_2}{\partial x_2} & \frac{\partial \dot{x}_2}{\partial x_3} \\ \frac{\partial \dot{x}_3}{\partial x_1} & \frac{\partial \dot{x}_3}{\partial x_2} & \frac{\partial \dot{x}_3}{\partial x_3} \end{bmatrix} = \begin{bmatrix} 0 & 1 & 0 \\ f_1 & f_2 & f_3 \\ 0 & 0 & -\frac{1}{RC} \end{bmatrix}.$$

The linearized state space equation is therefore

$$\begin{bmatrix} \dot{x}_1 \\ \dot{x}_2 \\ \dot{x}_3 \end{bmatrix} = \begin{bmatrix} 0 & 1 & 0 \\ f_1 & f_2 & f_3 \\ 0 & 0 & -\frac{1}{RC} \end{bmatrix} \begin{bmatrix} x_1 \\ x_2 \\ x_3 \end{bmatrix} + \begin{bmatrix} 0 \\ 0 \\ \frac{1}{RC} \end{bmatrix} u.$$
 (32)

It can be observed from the second state that the actuator acts as a spring-mass-damper system in series with the RC series circuit. $f_1 = \omega_n^2$ is the term that describes the natural frequency of the system. It is through f_1 that the stretch affects the dynamics of the system as seen in Appendix C. For this nonlinear problem, f_1 varies also with voltage hence in practice the spring constant is a variable parameter during

the actuation of the DEA. $f_2 = 2\zeta \omega_n$ serves as the damping term. This is where the viscous effects of the membrane affect the dynamics of the actuator. For a model without viscosity, $f_2 = 0$, which is true for the quasi-static model. $f_3 = Kf_1$ serves as the input gain from the voltage applied onto the membrane where K is the constant gain of the system. The overall gain, f_3/RC increases with increasing displacement and voltage. Also the gain will increase with a decreasing time constant. \dot{x}_1 and \dot{x}_2 make the second order system that is driven by \dot{x}_3 , a first order system for the RC series circuit of the tubular actuator whose time constant contributes to the control gain of the system. The expression of the transfer function of the voltage input u to the disk position x_1 is given as

$$G(s) = \frac{\frac{f_3}{RC}}{s^3 + (\frac{1}{RC} - f_2)s^2 - (f_1 + \frac{f_2}{RC})s - \frac{f_1}{RC}}.$$
 (33)

The parameters f_1 , f_2 , f_3 , and $\frac{1}{RC}$ can now be determined with frequency response analysis by inspecting the frequency response of the actuator over the range [0.02-8] Hz and fitting a transfer function onto the data. At this point one can trace how the physical parameters like stretch and the time constant of the actuator affect and interact with the actuator performance, control, and model. The model developed in this manner is thus unique.

3.2 Determining f_1 , f_2 , and f_3 analytically

In this section an attempt is made to determine f_1 , f_2 , and f_3 analytically by making some assumptions on the non-linear model to further simplify the process. Since the curvature of the DEA is small, the DEA shape is assumed to retain the un-stretched shape such that $\theta \approx 90^{\circ}$. r is also assumed to be constant such that $r \approx R$. This gives the acceleration \dot{x}_2 in the non-normalized form as

$$\dot{x}_2 = \frac{-2\pi H \mu R L^3}{m x_1^3} \left(\left[1 - \frac{\varepsilon x_3^2}{\mu H^2} \right] \frac{x_1^4}{L^4} - 1 \right) - \frac{c}{m} x_2.$$
 (34)

From this expression f_1 becomes

$$f_1 = \frac{-2\pi H \mu R}{mL} \left[-1 + \frac{\varepsilon}{H^2 \mu} x_3^2 - \frac{3}{\lambda_1^4} \right] \times 2\pi H \mu.$$
 (35)

 f_2 is given as

$$f_2 = -\frac{c}{m} \times 2\pi H \mu,\tag{36}$$

where the value of c is determined from the exponential decay of the tubular actuator. f_3 is determined using

$$f_3 = \frac{4\pi R\varepsilon}{mH} \lambda_1 x_3 \times 2\pi H\mu. \tag{37}$$

By inserting the operating point values of x_3 , λ_1 , and c, f_1 , f_2 , and f_3 can be determined.

3.3 Experimental Setup and Frequency Response Analysis

Figure 6 shows the experimental setup. A sinusoidal input signal of amplitude 2 kV running at a different frequency is used for each experiment. The output for the displacement magnitude of the DE tube is measured by the laser sensor (OADM 2016441/S14F) with units in millimeters (mm). A 20 gf load is placed on the free end of the DE tube. The actuation voltage is provided by a high voltage amplifier (20HVA24-P2-F). The geometric parameters of the tubular actuator are shown in Table 3. All data is collected using dSpace [38].

Table 3 DE tube geometry parameters

Parameter	Value	Unit
R	8.2	(mm)
H	0.52	(mm)
L	80	(mm)

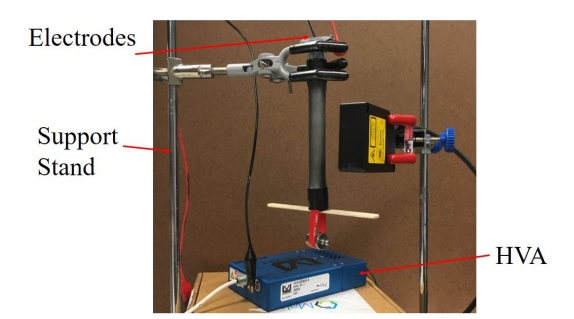


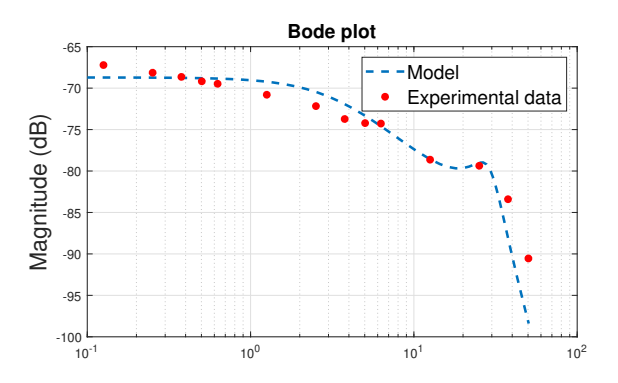
Fig. 6 Experimental setup.

A transfer function is estimated from the experimental data from which the values of f1, f2, f3, and 1/RC can be calculated. The transfer function is determined empirically by tuning the transfer function coefficients to fit the experimental data as close as possible. Figure 7 shows the bode diagram of the tubular actuator along with the experimental data. The transfer function of the tubular actuator is given as:

$$G(s) = \frac{1.1}{s^3 + 16s^2 + 900s + 3000}. (38)$$

The parameters f_1 , f_2 , f_3 , and $\frac{1}{RC}$ are thus determined as $f_1 = -856.2159$, $f_2 = -12.4962$, $f_3 = 0.3139$, and $\frac{1}{RC} = 3.5038$. The time constant τ for the electric circuit is therefore 0.2854 s. The state space model is:

$$\begin{bmatrix} \dot{x}_1 \\ \dot{x}_2 \\ \dot{x}_3 \end{bmatrix} = \begin{bmatrix} 0 & 1 & 0 \\ -856.2159 & -12.4962 & 0.3139 \\ 0 & 0 & -3.5038 \end{bmatrix} \begin{bmatrix} x_1 \\ x_2 \\ x_3 \end{bmatrix} + \begin{bmatrix} 0 \\ 0 \\ 3.5038 \end{bmatrix} u.$$
 (39)



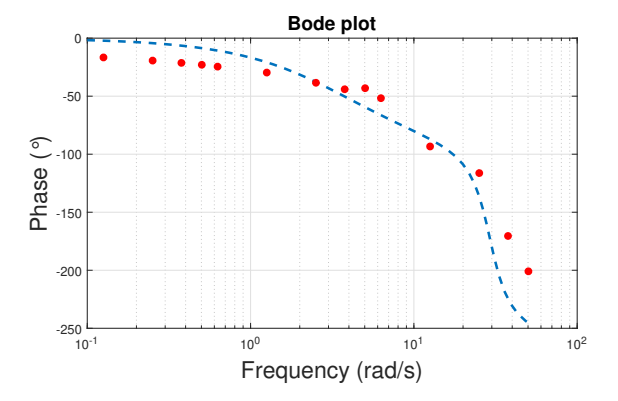


Fig. 7 Frequency response of the actuator.

For this setup, the operating point values are those used in running the frequency response of the actuator, $x_3 = 2000$ V and $\lambda_1 = 1.1127$. Taking $\mu = 76500$ and $\varepsilon = 5.6234 \times 10^{-11}$ the parameters are determined analytically as $f_1 = -870.0983$ and $f_3 = 0.3093$. This is in close agreement with those determined using the frequency response.

4 Control System Design

4.1 PID control

A PID controller is designed using the Simulink [39] PID tuner with the nominal model to meet the desired performance requirements of having a settling time within two seconds and zero overshoot. The focus of the tuner is set to balance between reference tracking and disturbance rejection. For further details see [40]. The controller that is identified is

$$K_{PID} = 2623 + \frac{7764}{s} - 196 \frac{9.18}{1 + \frac{9.18}{s}}. (40)$$

Note that the derivative filter coefficient, N = 9.18 is set to be higher than the bandwidth of the actuator which

is 3.592 rad/s. A performance gain of 1.43×10^{-5} is used for slow reference tracking while a gain of 2×10^{-4} is used for fast reference tracking.

$4.2~H_{\infty}$ Synthesis

An H_{∞} controller is also chosen to handle system uncertainties arising from the non-linearity of the actuator which is not captured by the linearized model. As a robust controller it can also reject external disturbance and reduce sensor noise. Figure 8 shows the schematic of the controller.

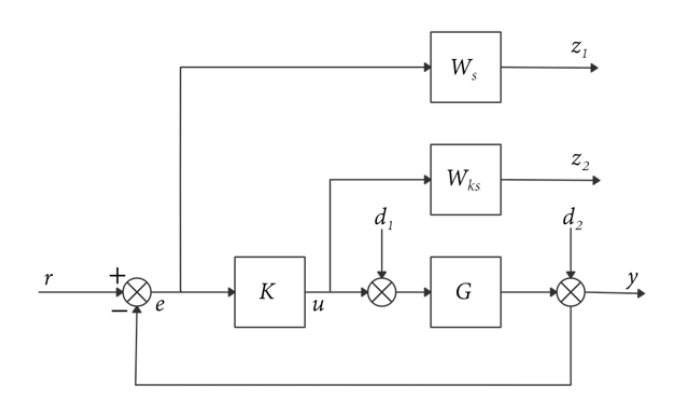


Fig. 8 Mixed sensitivity loop shaping for H_{∞} controller.

The reference signal is r, e is the error signal between the model output signal mixed with sensor noise d_2 , u is the control input from controller K, d_1 is the external disturbance that goes into the model G, W_s and W_{ks} are the error sensitivity weight and control sensitivity weight respectively while z_1 and z_2 are the corresponding performance signal outputs. In selecting the weights, the objective is to maintain good signal tracking and disturbance rejection which amounts to setting the sensitivity function, S small for low frequencies. The controller is also required to reject sensing noise and also account for model uncertainty, ΔG which amounts to setting the sensitivity function close to unity for high frequencies. As a results the weights are chosen as

$$W_s = \frac{0.2s + 6.283}{s + 0.0006283},$$

$$W_{ks} = \frac{0.0012s + 0.001508}{0.0001s + 6.283}.$$
(41)

$$W_{ks} = \frac{0.0012s + 0.001508}{0.0001s + 6.283}. (42)$$

The controller synthesized using these weights turns out to

$$K = \frac{68.07s^4 + 4.278 \times 10^6 s^3 + 6.849 \times 10^7 s^2 + 3.849 \times 10^9 s + 1.283 \times 10^{10}}{s^5 + 317.8s^4 + 6927s^3 + 2.951 \times 10^5 s^2 + 2.001 \times 10^6 s + 1257}.$$
(43)

The controller is of a higher order and is difficult to implement in real time control so a reduced order controller K_r is generated from K. The controller is obtained using the balred command in Matlab. The controller generated is given by

$$K_r = \frac{-34.99s^2 + 1.39 \times 10^4 s + 4.911 \times 10^4}{s^2 + 7.657s + 0.004811}.$$
 (44)

 K_r is further multiplied by a performance gain of 5×10^{-4} for fast reference tracking and a gain of 7×10^{-5} for slow reference tracking. The gains reduce the controller sensitivity and conserve control energy while controlling the tubular actuator.

To ensure internal stability of the system, M(s) in the presence of model uncertainty, the impact of ΔG on the overall system is analyzed. ΔG is added from the plant input to the plant output such that the true plant, $G_{true} = G + \Delta G$. Using small gain theory, the system is stable if $||M||_{\infty} < \frac{1}{||\Delta G||_{\infty}}$. From figure 8, $M = \frac{K}{1+KG}$ and $||M||_{\infty} = 2,778.86$. The model uncertainty is bounded by $\Delta G_b = \frac{0.063}{s^2 + 54s + 900}$. Figure 9 shows the modeled uncertainty used to bound the model error. Since $||\Delta G||_{\infty} < ||\Delta G_b||_{\infty} = 7 \times 10^{-5}$, the inter-

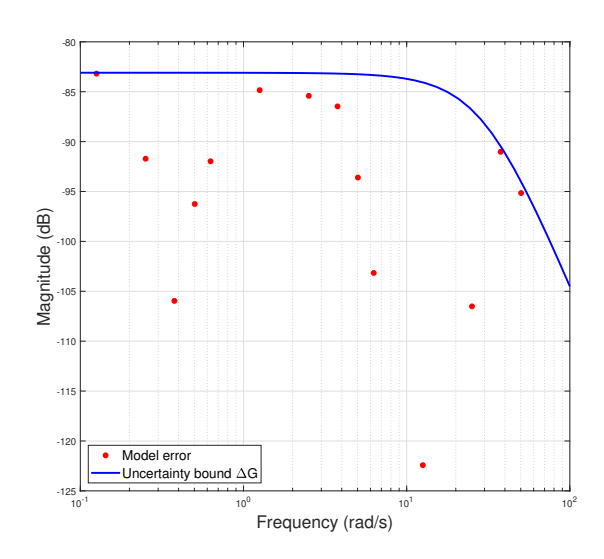


Fig. 9 Model uncertainty.

nal stability condition is met $||M||_{\infty} < \frac{1}{||\Delta G||_{\infty}} = 14,285.71$

5 Experimental Results

The controllers are implemented digitally via Simulink [39] in connection with dSpace to evaluate their performance. The sampling time for all the experiments carried out is 0.001 s. In comparing the performance of the controllers, they are evaluated based on the reference tracking error, e(mm)and control energy consumption, u(V). The performance for

both is evaluated using the root mean square (rms) value of the signals defined by

$$*rms = \sqrt{\frac{\Sigma(*)^2}{N}},\tag{45}$$

where * is the signal in question and N is the length of the signal (total number of elements in the signal). The controllers are tested on how well they reject external disturbances and reduce sensor noise.

The external disturbance introduced into the system may be treated as an impulse or pulse. It is generated by tapping on the stand that supports the tubular actuator and as a result causes it to swing back and forth. This causes an increase in the magnitude of the error signal that the controllers compensate for to maintain good reference tracking. Figures 10 and 11 show the results for position reference tracking of the tubular actuator using PID and H_{∞} control respectively for a 0.003 Hz sinusoidal reference while Figure 12 and 13 show the results for position reference tracking at higher frequencies of actuation for a sinusoidal reference of 1 Hz. Even with sensor noise, the controllers are able to track the reference signal but with a steady state error.

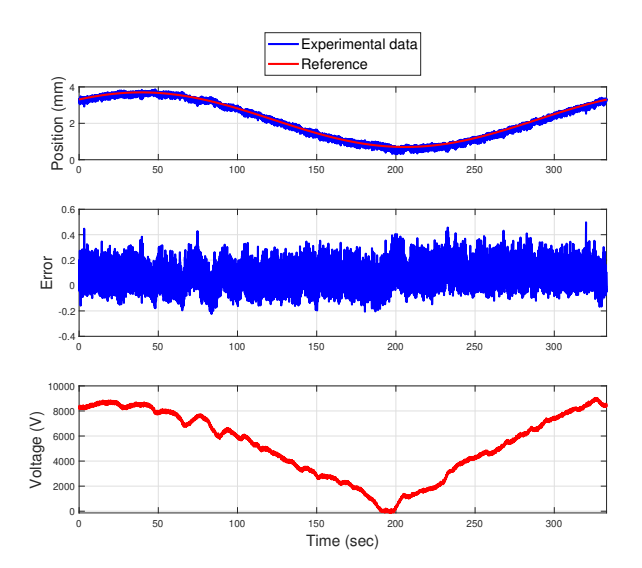
The reference tracking performance in terms of RMS at different frequencies and amplitudes without external disturbance is shown in figure 14. It is observed that H_{∞} performs better than the PID controller without any external disturbance. This is as expected due to the fact that in designing the H_{∞} controller, sensing noise is taken into account, this being a more robust controller. The control effort for both controllers is comparable as shown in figure 15.

When external disturbances are introduced, the PID controller performs better at higher frequency actuation while H_{∞} is better at lower frequency actuation as seen in figure 16. On the other hand the H_{∞} controller still conserves the control effort more than the PID controller as is shown in figure 17.

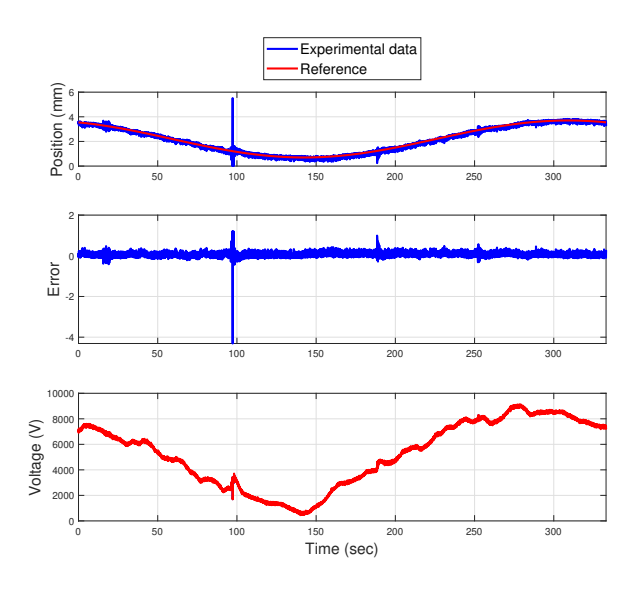
The difference in performance may be attributed to the fact that the gain used for the H_{∞} controller is high, making the controller sensitive and in effect causing the controller to use more control effort for better reference tracking and noise rejection than the PID controller. A lower gain might help the controller use even less control effort while still maintaining good reference tracking.

6 Conclusion and Future Work

In this exercise, it is shown how the quasi-static model can be converted into a dynamic model for control purposes. The dynamic model is linearized about an operating point and the parameters of the linearized model are determined analytically and experimentally. The analytic approach allows for fast adjustment and model update when the operating point of the actuator changes removing the need to run



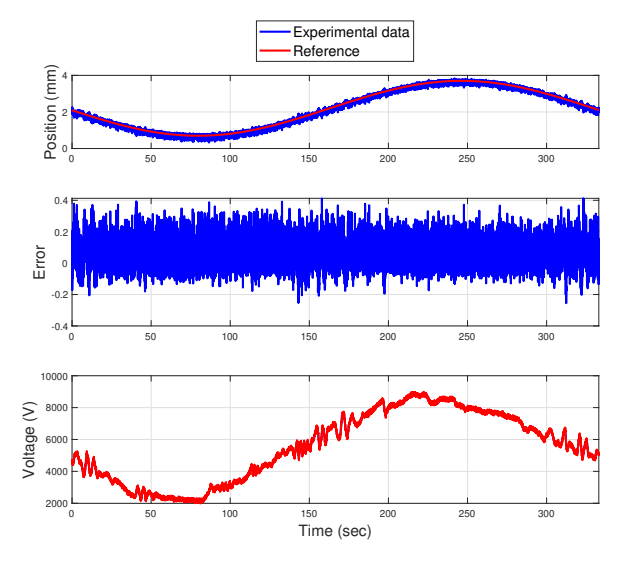
(a) 0.003 Hz sine wave without disturbance



(b) 0.003 Hz sine wave with disturbance

Fig. 10 0.003 Hz sinusoidal reference tracking using PID controller. (a) without disturbance (b) with disturbance around 20, 90, 190, and 250 s.

experiments each time in identifying these values. The influence of how the pre-stretch, applied voltage, and shear modulus affect the system is also shown. Reference tracking is finally performed to show that the non-linear tubular actuator can be controlled using PID and H_{∞} controls in the presence of sensing noise and external disturbance. The H_{∞} robust controller is designed to reduce on energy consumption while maintaining good reference tracking. The



(a) 0.003 Hz sine wave without disturbance

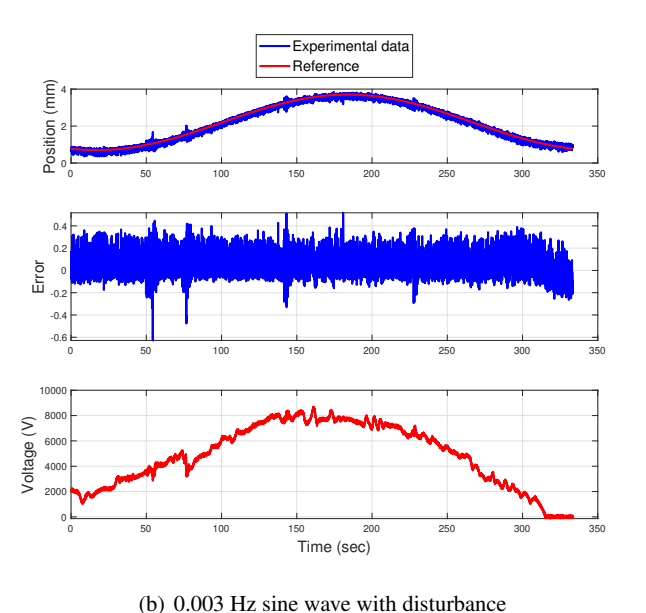
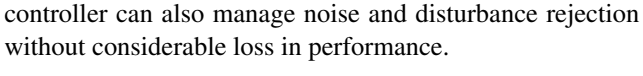


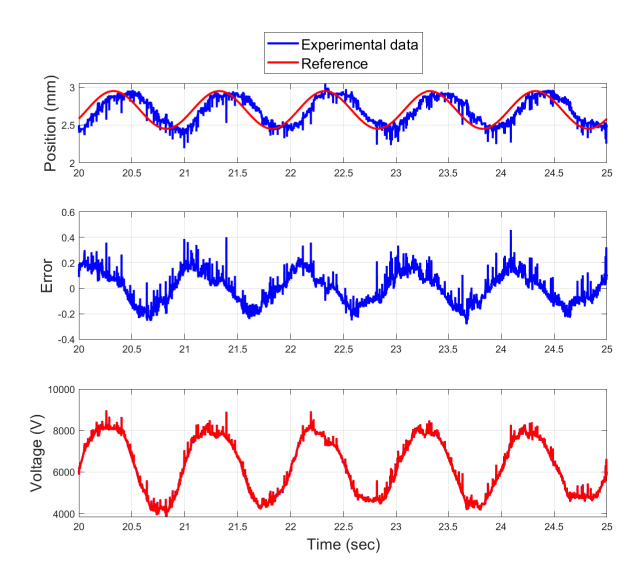
Fig. 11 0.003 Hz sinusoidal reference tracking results using H_{∞} con-

and 220 s.

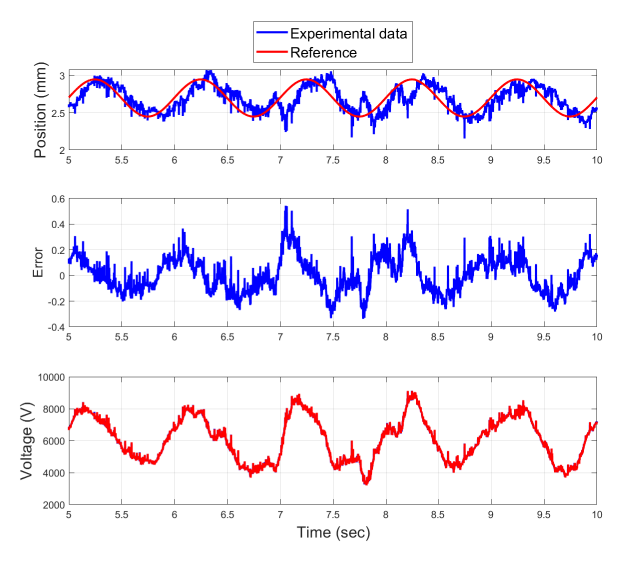


troller. (a) without disturbance (b) with disturbance around 50, 70, 140,

Future work has to be done in utilizing a more complex model to accurately predict displacements over large mechanical loads and strains as well as to account for membrane stiffening during actuation. The Gent, Ogden, and Yeoh models are good candidates to use as a model that can cover large stretch regions. Since the VHB dielectric elastomer membranes have high viscous effects, it is worth looking



(a) 1 Hz sine wave without disturbance

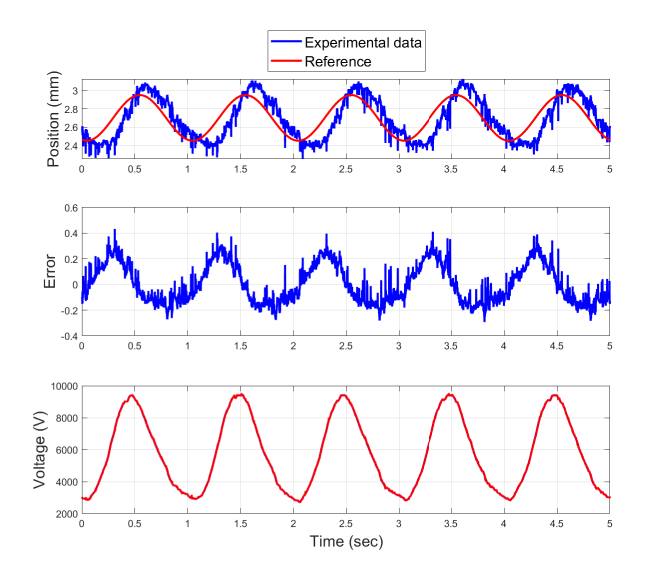


(b) 1 Hz sine wave with disturbance

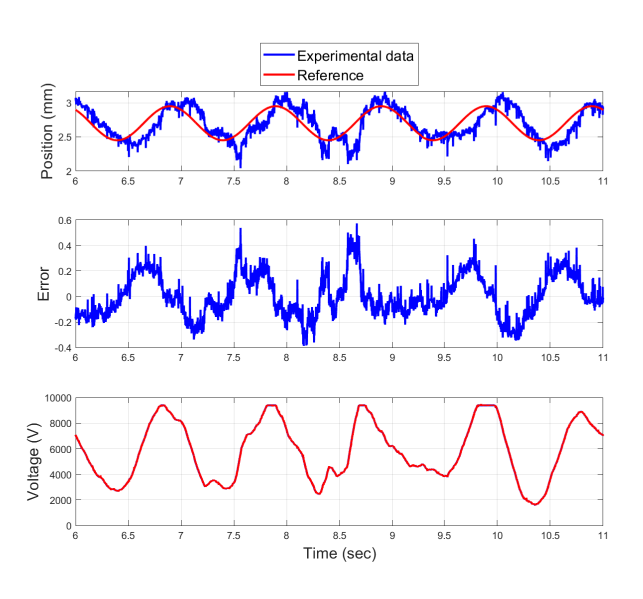
Fig. 12 $\,^1$ Hz sinusoidal reference tracking using PID controller. (a) without disturbance (b) with disturbance between 6 and 8.5 s.

into models that incorporate this effect with a relaxation term that affects the dynamics of the membrane with time during loading and unloading as well as with the frequency of the membrane actuation.

Acknowledgements This work was supported by the National Science Foundation under Grant CMMI #1747855.



(a) 1 Hz sine wave without disturbance



(b) 1 Hz sine wave with disturbance

Fig. 13 1 Hz sinusoidal reference tracking results using H_{∞} controller (a) without disturbance (b) with disturbance between 7 and 9 s.

APPENDIX

6.1 APPENDIX A: Derivation of Equations of State

Starting with Eqn. 10,

$$\delta E_H = 2\pi RH \int \delta W dX = F \delta z_B + \Phi \delta Q.$$

Here,

$$\int \delta W dX = \int (s_1 \delta \lambda_1 + s_2 \delta \lambda_2 + \bar{E} \delta \bar{D}) dX. \tag{46}$$

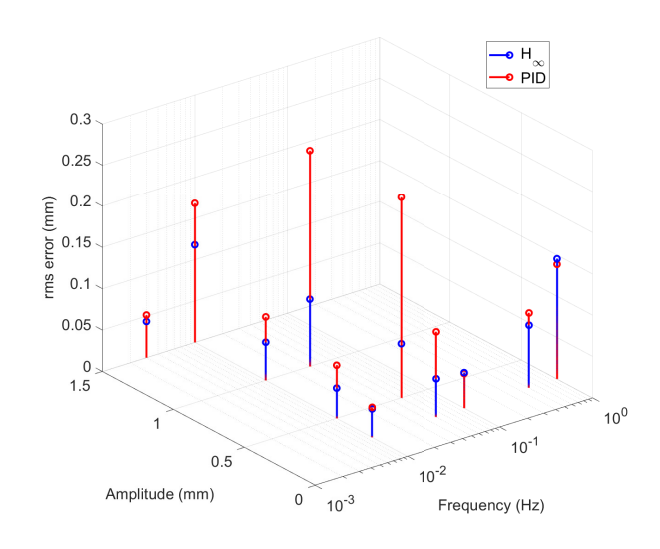


Fig. 14 Comparison of tracking error with no external disturbance applied.

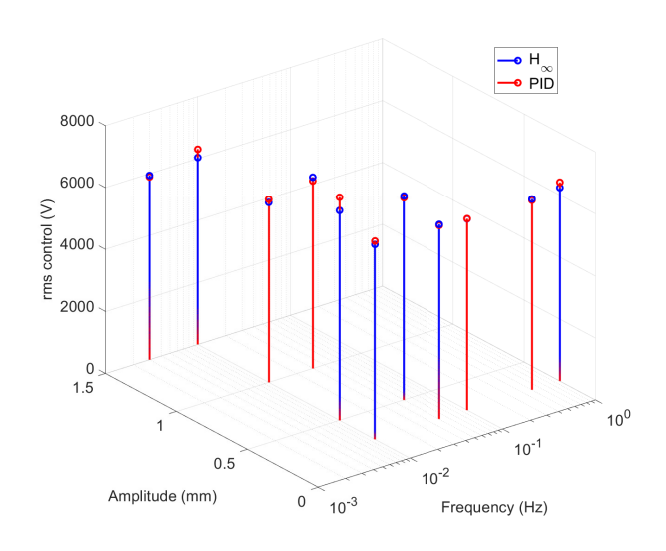


Fig. 15 Comparison of control effort without external disturbance.

A small change in λ_1 is given by

$$\delta \lambda_1 = \frac{\partial \lambda_1}{\partial dl} \delta dl = \frac{\delta dl}{dX} \tag{47}$$

and from Eqn. 2, taking a small change in dl

$$\delta dl = \frac{dr}{dl} \delta dr + \frac{dz}{dl} \delta dz.$$

Substituting Eqn. 1 into this result gives

$$\delta dl = -\cos\theta \delta dr + \sin\theta \delta dz.$$

Finally Eq. 47 is written as

$$\delta \lambda_1 = -\cos\theta \frac{d(\delta r)}{dX} + \sin\theta \frac{d(\delta z)}{dX}.$$
 (48)

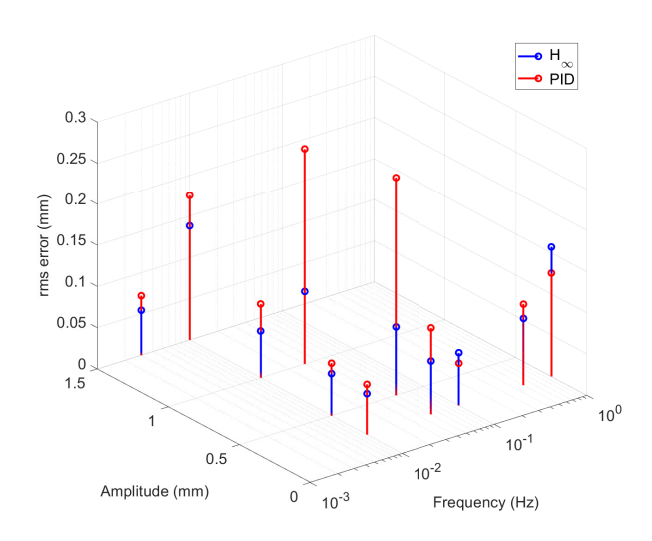


Fig. 16 Comparison of tracking error with external disturbance.

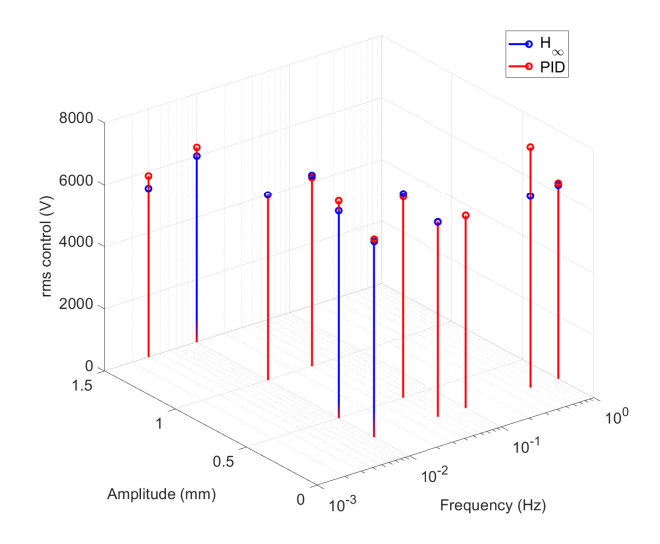


Fig. 17 Comparison of control effort with external disturbance.

Also a small change in λ_2 is given by

$$\delta \lambda_2 = \frac{\partial \lambda_2}{\partial r} \delta r = \frac{\delta r}{R}.$$
 (49)

Finally, from Eqn. 5, a small change in \bar{D} is given by

$$\delta \bar{D} = \frac{\delta q}{A_0}.\tag{50}$$

With these, Eqn. 46 becomes

$$\int \left[s_1 \left(-\cos\theta \frac{d(\delta r)}{dX} + \sin\theta \frac{d(\delta z)}{dX} \right) + s_2 \frac{\delta r}{R} + \bar{E} \frac{\delta q}{A_0} \right] dX$$

$$= \int \left[-s_1 \cos\theta \frac{d(\delta r)}{dX} + s_1 \sin\theta \frac{d(\delta z)}{dX} + s_2 \frac{\delta r}{R} + \bar{E} \frac{\delta q}{A_0} \right] dX.$$

Integrating by parts gives

$$s_{1}(-\cos\theta\delta r + \sin\theta\delta z)\Big|_{A}^{B} + \int \left[\left(\frac{d(s_{1}\cos\theta)}{dX} + \frac{s_{2}}{R}\right)\delta r - \frac{d(s_{1}\sin\theta)}{dX}\delta z + \bar{E}\frac{\delta q}{A_{0}}\right]dX.$$

By comparing the left hand side with the right hand side of the equation, the following is observed from the δz term inside the integral

$$\frac{d(s_1 \sin \theta)}{dX} = 0 \qquad \Longrightarrow s_1 \sin \theta = Constant. \tag{51}$$

Since there is no δz on the right hand side, physically this means that the vertical longitudinal stress component is fixed for a given applied load. This is the expected condition for the membrane in static equilibrium since the vertical force components must cancel out each other. Evaluating the boundaries gives

$$2\pi RH \left\{ s_1(-\cos\theta_B \delta r_B + \sin\theta_B \delta z_B) - s_1(-\cos\theta_A \delta r_A + \sin\theta_A \delta z_A) \right\} = F \delta z_B.$$

The boundary conditions for the tubular actuator require that $\delta r_B = \delta r_A = \delta z_A = 0$. Therefore

$$2\pi R H s_1 \sin \theta_B \delta z_B = F \delta z_B$$

$$2\pi R H s_1 \sin \theta = F.$$
(52)

This corresponds to Eqn. 15. Moving back into the integral is Eqn. 14 directly from

$$\frac{d(s_1 \cos \theta)}{dX} + \frac{s_2}{R} = 0$$

$$\frac{d(s_1 \cos \theta)}{dX} = -\frac{s_2}{R}.$$
(53)

This result is from the fact that there are no external forces acting on the surface of the membrane radially as would be the case if the actuator were to be under compression or tension by an applied pressure on the membrane [41]. Finally,

$$2\pi RH \int \bar{E} \frac{\delta q}{A_0} dX = \Phi \delta Q.$$

Taking the actuator as a cylindrical capacitor, \bar{E} does not vary along the longitudinal direction and hence is a constant with respect to the X-direction. This gives

$$H\bar{E}\cdot 2\pi R\int \frac{\delta q}{A_0}dX = \Phi \delta Q.$$

And from Eqn. 6

$$\delta Q = 2\pi R \int \frac{\delta q}{A_0} \tag{54}$$

herefore

$$H\bar{E} = \Phi. \tag{55}$$

6.2 APPENDIX B: Derivation of the governing differential equations

This is the extended derivation of equations 21 to 23: Divide Eqn. 1 by dX to get

$$\frac{dr}{dX} = -\frac{dl}{dX}\cos\theta, \qquad \qquad \frac{dz}{dX} = -\frac{dl}{dX}\sin\theta.$$

But $\frac{dl}{dX} = \lambda_1$. This gives Eqn. 21 which is

$$\frac{dr}{dX} = -\lambda_1 \cos \theta, \qquad \qquad \frac{dz}{dX} = \lambda_1 \sin \theta.$$

Using Eqn. 14 and 51 one can get Eqn. 22. Solving Eqn. 14 gives

$$\frac{ds_1}{dX}\cos\theta = s_1\sin\theta \frac{d\theta}{dX} - \frac{s_2}{R} \tag{56}$$

and solving Eqn. 51 gives

$$\frac{ds_1}{dX}\sin\theta = -s_1\cos\theta\frac{d\theta}{dX}.$$
 (57)

Dividing Eqn. 57 by Eqn. 56 gives

$$\tan \theta = \frac{-s_1 \cos \theta \frac{d\theta}{dX}}{s_1 \sin \theta \frac{d\theta}{dX} - \frac{s_2}{R}}.$$

Solving for $\frac{d\theta}{dX}$ gives

$$s_1 (\tan \theta \cdot \sin \theta + \cos \theta) \frac{d\theta}{dX} = \frac{s_2}{R} \tan \theta$$
$$s_1 \frac{d\theta}{dX} = \frac{s_2}{R} \sin \theta$$

Expanding $\tan \theta$ gives

$$s_1 \left(\frac{\sin \theta}{\cos \theta} \cdot \sin \theta + \cos \theta \right) \frac{d\theta}{dX} = \frac{s_2}{R} \tan \theta,$$
$$s_1 \left(\frac{\sin^2 \theta + \cos^2 \theta}{\cos \theta} \right) \frac{d\theta}{dX} = \frac{s_2}{R} \tan \theta,$$

and using the trigonometric identity $\sin^2 \theta + \cos^2 \theta = 1$ and multiplying through by $\frac{\cos \theta}{\sin^2 \theta}$ gives us Eqn. 22 as

$$\frac{d\theta}{dX} = \frac{s_2}{s_1 R} \sin \theta. \tag{58}$$

Now the algebraic equation 23 can be derived by solving for s_1 in Eqn. 15 and Eqn. 18 and setting the two equations equal to each other. From Eqn. 15

$$s_1 = \frac{F}{2\pi R H \sin \theta}.$$

Using the normalized load F^* gives

$$s_1 = \frac{\mu F^*}{R \sin \theta}$$

and with Eqn. 18

$$\begin{split} s_1 &= \mu \left(\lambda_1 - \frac{1}{\lambda_1^3 \lambda_2^2} \right) - \frac{\bar{D}^2}{\varepsilon \lambda_1^3 \lambda_2^2} = \frac{\mu F^*}{R \sin \theta} \\ &\frac{\mu \varepsilon \lambda_1^4 \lambda_2^2 - \mu \varepsilon - \bar{D}^2}{\varepsilon \lambda_1^3 \lambda_2^2} = \frac{\mu F^*}{R \sin \theta}. \end{split}$$

From Eqn. 20, $\bar{D} = \varepsilon \lambda_1^2 \lambda_2^2 \bar{E}$ so,

$$\frac{\mu \varepsilon \lambda_1^4 \lambda_2^2 - \mu \varepsilon - \varepsilon^2 \lambda_1^4 \lambda_2^4 \bar{E}^2}{\varepsilon \lambda_1^3 \lambda_2^2} = \frac{\mu F^*}{R \sin \theta}$$
$$\lambda_1^4 \left(1 - \frac{\varepsilon \bar{E}^2}{\mu} \lambda_2^2 \right) - \frac{1}{\lambda_2^2} = \frac{F^*}{R \sin \theta} \lambda_1^3$$

From Eqn. 16, $\bar{E}^2 = \frac{\Phi^2}{H^2}$. Substituting this in the above expression gives

$$\lambda_1^4 \left(1 - \frac{\varepsilon}{\mu} \cdot \frac{\bar{\Phi}^2}{H^2} \lambda_2^2 \right) - \frac{1}{\lambda_2^2} = \frac{F^*}{R \sin \theta} \lambda_1^3$$

Using the normalized applied voltage on the membrane gives the algebraic equation

$$\left[1 - \left(\frac{\Phi^* r}{R}\right)^2\right] \lambda_1^4 - \frac{F^*}{R \sin \theta} \lambda_1^3 - \left(\frac{R}{r}\right)^2 = 0.$$
 (59)

6.3 APPENDIX C: Jacobian elements

$$\frac{\partial \dot{x}_1}{\partial x_1} = 0,$$
 $\frac{\partial \dot{x}_1}{\partial x_2} = 1,$ $\frac{\partial \dot{x}_1}{\partial x_2} = 0.$

$$\begin{split} f_1 &= \frac{\partial \dot{x}_2}{\partial x_1} = \frac{1}{m} \left\{ R \cos \theta \left(\left[1 - \left(\frac{x_3^* r}{R} \right)^2 \right] \lambda_1 - \frac{R^2}{r^2 \lambda_1^3} \right) \frac{\partial \theta}{\partial x_1} \right. \\ &+ 2R \sin \theta \left(\frac{R^2}{r^3 \lambda_1} - \frac{r \lambda_1 x_3^2}{R^2} \right) \frac{\partial r}{\partial x_1} \\ &+ R \sin \theta \left(1 - \left(\frac{x_3^* r}{R} \right)^2 + \frac{3R^2}{r \lambda_1^4} \right) \frac{\partial \lambda_1}{\partial x_1} \right\}, \end{split}$$

$$f_2 = \frac{\partial \dot{x}_2}{\partial x_2} = -\frac{c^*}{m},$$

$$f_3 = \frac{\partial \dot{x}_2}{\partial x_3} = \frac{2r^2\lambda_1 x_3^*}{mR} \sin \theta,$$

and

$$\frac{\partial \dot{x}_3}{\partial x_1} = 0, \qquad \qquad \frac{\partial \dot{x}_3}{\partial x_2} = 0, \qquad \qquad \frac{\partial \dot{x}_3}{\partial x_3} = -\frac{1}{RC}.$$

References

- P. Brochu and Q. Pei, "Advances in dielectric elastomers for actuators and artificial muscles," *Macromolecular rapid communications*, vol. 31, pp. 10–36, 01 2010.
- L. Romasanta, M. Lopez-Manchado, and R. Verdejo, "Increasing the performance of dielectric elastomer actuators A review from the materials perspective," *Progress in Polymer Science*, vol. 51, pp. 188–211, 2015, environmentally Relevant and Hybrid Polymer Materials. [Online]. Available: https://www.sciencedirect.com/science/article/pii/S0079670015000921
- H. Stoyanov, P. Brochu, X. Niu, C. Lai, S. Yun, and Q. Pei, "Long lifetime, fault-tolerant freestanding actuators based on a silicone dielectric elastomer and self-clearing carbon nanotube compliant electrodes," RSC Adv., vol. 3, pp. 2272–2278, 2013. [Online]. Available: http://dx.doi.org/10.1039/C2RA22380E
- R. K. Katzschmann, J. DelPreto, R. MacCurdy, and D. Rus, "Exploration of underwater life with an acoustically controlled soft robotic fish," *Science Robotics*, vol. 3, no. 16, 2018.
- A. Marchese, C. Onal, and D. Rus, "Autonomous soft robotic fish capable of escape maneuvers using fluidic elastomer actuators," *Soft Robotics*, vol. 1, pp. 75–87, 03 2014.
- R. Pelrine, R. Kornbluh, Q. Pei, S. Stanford, S. oh, J. Eckerle, and K. Meijer, "Dielectric elastomer artificial muscle actuators: Toward biomimetic motion," *Proc. SPIE*, vol. 4695, pp. 126–137, 07 2002.
- C. Jordi, S. Michel, and E. Fink, "Fish-like propulsion of an airship with planar membrane dielectric elastomer actuators," *Bioin*spiration & biomimetics, vol. 5, p. 026007, 06 2010.
- F. Carpi, S. Bauer, and D. de rossi, "Stretching dielectric elastomer performance," *Science (New York, N.Y.)*, vol. 330, pp. 1759–61, 12 2010
- R. Pelrine, P. Sommer-Larsen, R. D. Kornbluh, R. Heydt, G. Kofod, Q. Pei, and P. Gravesen, "Applications of dielectric elastomer actuators," in *Smart Structures and Materials 2001: Electroactive Polymer Actuators and Devices*, Y. Bar-Cohen, Ed., vol. 4329, International Society for Optics and Photonics. SPIE, 2001, pp. 335 349.
- R. Pelrine, R. D. Kornbluh, J. Eckerle, P. Jeuck, S. Oh, Q. Pei, and S. Stanford, "Dielectric elastomers: generator mode fundamentals and applications," in *Smart Structures and Materials 2001: Elec*troactive Polymer Actuators and Devices, Y. Bar-Cohen, Ed., vol. 4329, International Society for Optics and Photonics. SPIE, 2001, pp. 148 – 156.
- G. Kovacs, P. Lochmatter, and M. Wissler, "An arm wrestling robot driven by dielectric elastomer actuators," *Smart Material Structures*, vol. 16, pp. 306–, 04 2007.
- B. Massa, S. Roccella, M. C. Carrozza, and P. Dario, "Design and development of an underactuated prosthetic hand." in *Proceedings ICRA* '02, *IEEE International Conference on Robotics and Automation*, vol. 4, 01 2002, pp. 3374–3379.
- P. Chakraborti, H. K. Toprakci, P. Yang, N. D. Spignal, P. Franzon, and T. Ghosh, "A compact dielectric elastomer tubular actuator for refreshable braille displays," *Sensors and Actuators A: Physical*, vol. 179, pp. 151 – 157, 2012.
- M. Tryson, H.-E. Kiil, and M. Benslimane, "Powerful tubular core free dielectric electro activate polymer (DEAP) push actuator," in *Electroactive Polymer Actuators and Devices (EAPAD)* 2009, Y. Bar-Cohen and T. Wallmersperger, Eds., vol. 7287, International Society for Optics and Photonics. SPIE, 2009, pp. 447 – 457. [Online]. Available: https://doi.org/10.1117/12.815740
- R. Sarban, R. Jones, B. Mace, and E. Rustighi, "A tubular dielectric elastomer actuator: Fabrication, characterization and active vibration isolation," *Mechanical Systems and Signal Processing*, vol. 25, no. 8, pp. 2879 2891, 2011.
- J.-S. Plante and S. Dubowsky, "Large-scale failure modes of dielectric elastomer actuators," *International Journal of Solids and Structures - INT J SOLIDS STRUCT*, vol. 43, 04 2006.

- R. Sarban, B. Lassen, and M. Willatzen, "Dynamic electromechanical modeling of dielectric elastomer actuators with metallic electrodes," *IEEE/ASME Transactions on Mechatronics*, vol. 17, no. 5, pp. 960–967, Oct 2012.
- R. Sarban and R. W. Jones, "Physical model-based active vibration control using a dielectric elastomer actuator," *Journal of Intelli*gent Material Systems and Structures, vol. 23, no. 4, pp. 473–483, 2012.
- R. van Kessel, P. Bauer, and J. A. Ferreira, "Electrical modeling of cylindrical dielectric elastomer transducers," *Smart Materials* and *Structures*, vol. 30, no. 3, p. 035021, feb 2021. [Online]. Available: https://doi.org/10.1088/1361-665x/abde4f
- P. Huang, J. Wu, P. Zhang, Y. Wang, and C.-Y. Su, "Dynamic modeling and tracking control for dielectric elastomer actuator with model predictive controller," *IEEE Transactions on Indus*trial Electronics, pp. 1–1, 2021.
- G.-Y. Gu, U. Gupta, J. Zhu, L.-M. Zhu, and X. Zhu, "Modeling of viscoelastic electromechanical behavior in a soft dielectric elastomer actuator," *IEEE Transactions on Robotics*, vol. 33, no. 5, pp. 1263–1271, 2017.
- G. Rizzello, D. Naso, A. York, and S. Seelecke, "Closed loop control of dielectric elastomer actuators based on self-sensing displacement feedback," *Smart Materials and Structures*, vol. 25, no. 3, p. 035034, feb 2016.
- ——, "Closed loop control of dielectric elastomer actuators based on self-sensing displacement feedback," Smart Materials and Structures, vol. 25, no. 3, p. 035034, 02 2016.
- 24. Z. Ye, Z. Chen, R. Asmatulu, and H. Chan, "Robust control of dielectric elastomer diaphragm actuator for human pulse signal tracking," *Smart Materials and Structures*, vol. 26, no. 8, p. 085043, jul 2017. [Online]. Available: https://doi.org/10.1088/1361-665x/aa75f7
- S. Xie, P. Ramson, D. Graaf, E. Calius, and I. Anderson, "An adaptive control system for dielectric elastomers," in 2005 IEEE International Conference on Industrial Technology, 2005, pp. 335–340.
- T. Hoffstadt and J. Maas, "Adaptive sliding-mode position control for dielectric elastomer actuators," *IEEE/ASME Transactions on Mechatronics*, vol. 22, no. 5, pp. 2241–2251, 2017.
- G. Kovacs, L. Düring, S. Michel, and G. Terrasi, "Stacked dielectric elastomer actuator for tensile force transmission," *Sensors and Actuators A: Physical*, vol. 155, no. 2, pp. 299 307, 2009.
- Z. Ye and Z. Chen, "Modeling and control of 2-dof dielectric elastomer diaphragm actuator," *IEEE/ASME Transactions on Mechatronics*, vol. PP, pp. 1–1, 01 2019.
- G.-K. Lau, H.-T. Lim, J.-Y. Teo, and Y.-W. Chin, "Lightweight mechanical amplifiers for rolled dielectric elastomer actuators and their integration with bio-inspired wing flappers," *Smart Materials* and *Structures*, vol. 23, no. 2, p. 025021, jan 2014.
- S. Wang, T. Kaaya, and Z. Chen, "Self-sensing of dielectric elastomer tubular actuator with feedback control validation," Smart Materials and Structures, 2020.
- 31. T. He, L. Cui, C. Chen, and Z. Suo, "Nonlinear deformation analysis of a dielectric elastomer membrane–spring system," *Smart Materials and Structures*, vol. 19, no. 8, p. 085017, 07 2010.
- 32. B. Kim, S. B. Lee, J. Lee, S. Cho, H. Park, S. Yeom, and S. Park, "A comparison among neo-hookean model, mooney-rivlin model, and ogden model for chloroprene rubber," *International Journal of Precision Engineering and Manufacturing*, vol. 13, 05 2012.
- O. H. Yeoh, "Characterization of elastic properties of carbonblack-filled rubber vulcanizates," *Rubber Chemistry and Technol*ogy, vol. 63, no. 5, pp. 792–805, 1990.
- R. W. Ogden, "Large deformation isotropic elasticity on the correlation of theory and experiment for incompressible rubberlike solids," *Proceedings of the Royal Society of London. Series A, Mathematical and Physical Sciences*, vol. 326, no. 1567, pp. 565–584, 1972.

35. N. S. Nise, CONTROL SYSTEMS ENGINEERING, (With CD). John Wiley & Sons, 2007.

- 36. T. Lu, J. Huang, C. Jordi, G. Kovacs, R. Huang, D. R. Clarke, and Z. Suo, "Dielectric elastomer actuators under equal-biaxial forces, uniaxial forces, and uniaxial constraint of stiff fibers," *Soft Matter*, vol. 8, no. 22, pp. 6167–6173, 2012.
- MATLAB, 9.7.0.1216025 (R2019b). Natick, Massachusetts: The MathWorks Inc., 2019.
- 38. "dspace." [Online]. Available: https://www.dspace.com/en/inc/home.cfm
- S. Documentation, "Simulation and model-based design," 2020. [Online]. Available: https://www.mathworks.com/products/simulink.html
- 40. "Pid tuner app." [Online]. Available: https://www.mathworks.com/help/slcontrol/gs/automated-tuning-of-simulink-pid-controller-block.html
- S. Son and N. Goulbourne, "Dynamic response of tubular dielectric elastomer transducers," *International Journal of Solids and Structures*, vol. 47, no. 20, pp. 2672 2679, 2010.